CHEMISTRY OF MATERIALS

ARTICLE

pubs.acs.org/cm

Advanced Anticorrosive Coatings Prepared from the Mimicked Xanthosoma Sagittifolium-leaf-like Electroactive Epoxy with Synergistic Effects of Superhydrophobicity and Redox Catalytic Capability

Chang-Jian Weng,[†,‡] Chi-Hao Chang,[†,‡] Chih-Wei Peng,[†,‡] Shao-Wen Chen,[†,‡] Jui-Ming Yeh,[*,†,‡] Ching-Ling Hsu,[‡,§] and Yen Wei[⊥]

[†]Department of Chemistry, [§]Department of Physics, and [‡]Center for Nanotechnology, Chung-Yuan Christian University, Chung Li 32023, Taiwan, R. O. C

[⊥]Department of Chemistry, Drexel University, Philadelphia, Pennsylvania 19104, United States

ABSTRACT: Novel anticorrosion coating materials were prepared by replicating fresh plant leaves; these materials had a synergistic effect of superhydrophobicity and redox catalytic capability. Superhydrophobic electroactive epoxy (SEE) coating applied for corrosion protection was prepared and coated on the surface of cold-rolled steel (CRS) using a nanocasting technique from the surface structure of fresh Xanthosoma sagittifolium leaves. First, the transparent PDMS template was replicated from the surface structure of fresh Xanthosoma sagittifolium. Subsequently, the SEE coating was fabricated on the CRS electrode using a nanocasting technique with a transparent PDMS template and an electroactive-epoxy polymer solution as the ink. The CRS electrode coated with SEE was found to have a water contact angle (CA) of 153°, which was significantly higher than the smooth electroactive epoxy (EE) coated on the CRS by spin coating (CA = 81°). The SEE coating material not only shows superior water repellent properties but also has electroactive properties. It should be noted that the CRS coated with SEE was found to exhibit remarkably enhanced corrosion protection as compared to the corresponding CRS coated with a smooth counterpart, on the basis of a series of electrochemical corrosion measurements performed under saline conditions.

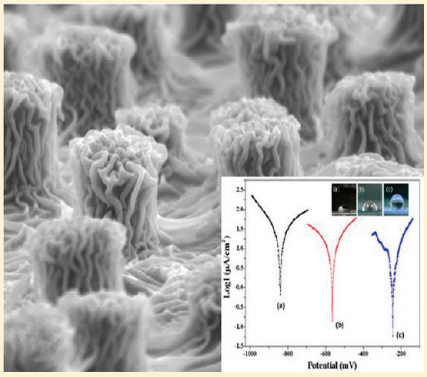

KEYWORDS: nanoimprinting, superhydrophobic surfaces, electroactive, lotus effect, epoxy, corrosion

INTRODUCTION

Corrosion control is an important subject of increasing interest to the modern metallic finishing industry. Many organic and/or polymeric coatings are designed to protect metal from in-service corrosion. One of the current industrial practices for anticorrosion is to treat the surface of metals with chromium-containing compounds. However, there are concerns regarding the known adverse health and environmental effects of chromium compounds.

In the past decade, some academic literatures reported that polyaniline (PANI) coatings revealed better anticorrosion properties on metallic substrates than several polymers.[1−5] A mechanism for enhanced corrosion protection of conjugated PANI coatings has been suggested to include the formation of a protective passivation oxide layer induced from the redox catalytic (i.e., electroactivity) capability of PANI.[6−9] Currently, aniline oligomer-derivating electroactive polymers[10] have attracted considerable research attention. For example, the preparation and electrochemical behavior of electroactive polyimides have been reported by Wang et al.[11,12] Furthermore, the electrochemical behaviors of electroactive polyamides with amine-capped aniline pentamers prepared by oxidative coupling polymerization have also been demonstrated by Zhang and co-workers.[13−17] Lately, Yeh and co-workers have reported the study of corrosion protection effects of polymer containing amine-capped aniline trimers coated on cold-rolled steel (CRS) electrodes.[18,19]

Over the past few years, the remarkable surface structures of superhydrophobic plant leaves, characterized by the so-called "lotus effect," have attracted the attention of many researchers.[20−22] In particular, the superhydrophobic property induced by these structures has become quite an important issue since there are a variety of practical applications utilizing their self-cleaning,[23] antifogging,[24] anticorrosive effects, etc.[25,26] In this regard, various methods involving the use of gel-like porous surfaces using polypropylene,[27] fibrous surfaces,[28,29] plasma-treated surfaces,[30,31] surfaces replicated from templates,[32,33] and rough block copolymer surfaces,[34,35] have been reported to produce artificial superhydrophobic surfaces.[36−42]

However, to the best of our knowledge, reports on the corrosion protection studies associated with superhydrophobic surfaces using electroactive polymer coatings are limited.

Received: October 22, 2010
Revised: March 18, 2011
Published: April 01, 2011

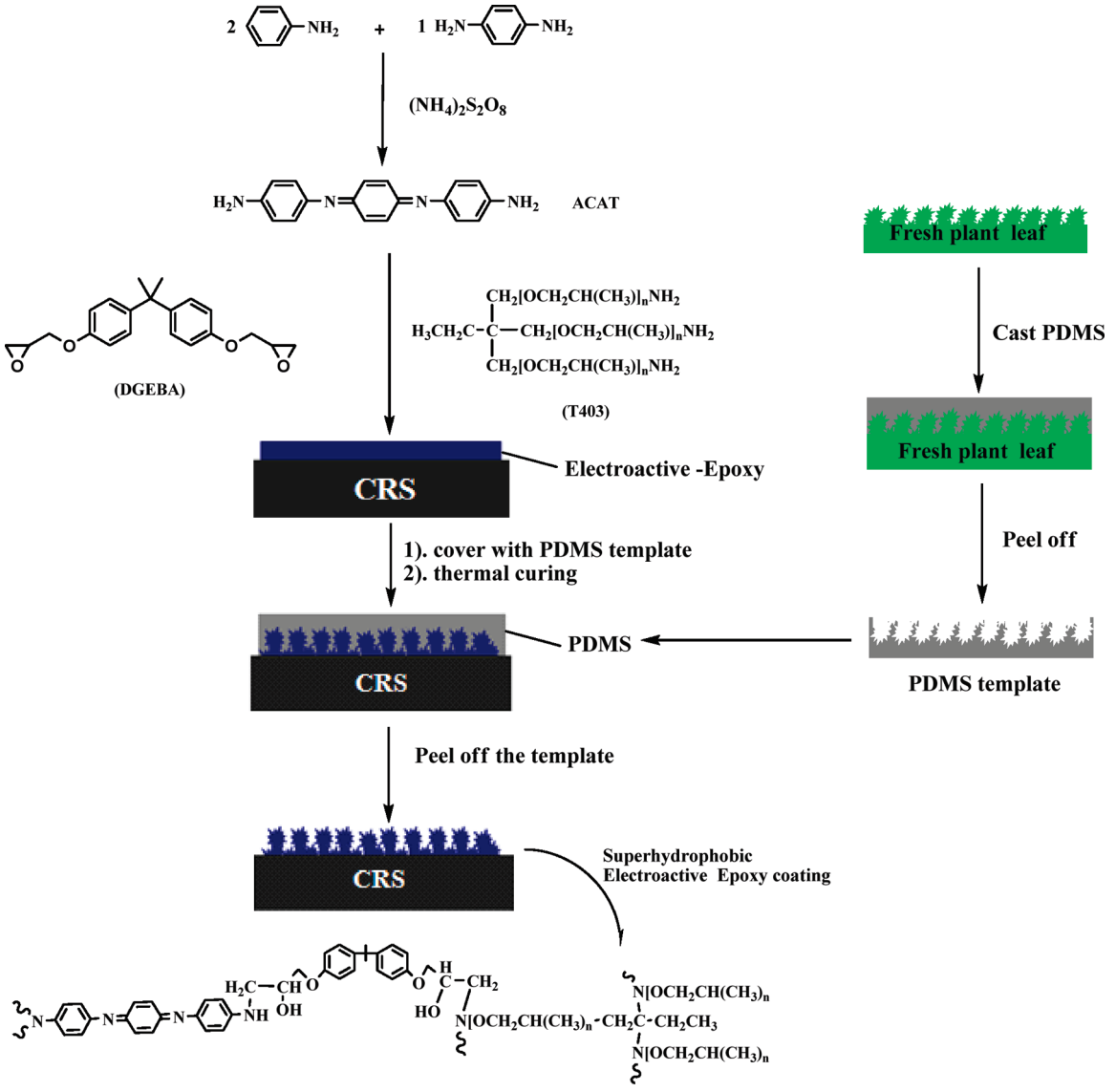

Figure 1. Scheme for the synthesis of superhydrophobic electroactive epoxy (SEE) coating materials.

Herein, we envisioned that the electroactive polymer surfaces with nanostructured surfaces might reveal enhanced corrosion protection, which may be attributed to the synergistic effect of a passive metal oxide layer induced from the electroactive polymer and the water repellent property from the morphology of the nanostructures. Therefore, in this work, we present the first preparation of superhydrophobic electroactive epoxy (SEE) coating materials using a nanocasting approach to fabricate superhydrophobic surfaces from Xanthosoma Sagittifolium leaves, and we evaluate their water repellent properties using contact angle. The corrosion protection effect on cold-rolled steel (CRS) electrodes based on a series of electrochemical corrosion was measured under saline conditions. The passivation oxide layer can be evaluated using SEM and ESCA.

EXPERIMENTAL SECTION

Chemicals and Instrumentations. Aniline (Sigma-Aldrich) was distilled prior to use. 1,4-phenylenediamine (Sigma-Aldrich), trimethylolpropane tris[poly-(propylene glycol) amine terminated] ether (T-403,Aldrich), bisphenol A diglycidyl ether (DGEBA, Aldrich), N,N-dimethylacetamide (DMAc), and polydimethylsiloxane (PDMS, Dow Corning, Sylgard 184) were used as received without further purification. All the reagents were reagent grade unless otherwise stated.

Mass spectra were run on a Bruker Daltonics IT mass spectrometer model Esquire 2000 (Leipzig, German) with an Agilent ESI source (model G1607−6001). ^{1}H NMR spectra were run on a Bruker 300 spectrometer, referenced to internal standard of tetramethylsilane (TMS), DMSO was used as solvent. Attenuated total reflectance FTIR spectra was obtained at a resolution of 4.0 cm^{-1} with a FT/IR spectrometer (FT/IR-4100) at room temperature ranged from 4000 to 650 cm^{-1}. The surface morphology of coating materials and passivation metal oxide layers were characterized by scanning electron microscopy (SEM), (Hitachi S-2300). The three-dimensional morphology of the surface were character by atomic force microscopy (AFM), (Park systems XE-100). Contact angles of samples were measured using a First Ten Angstroms FTA 125. Electron spectroscopy was measured by chemical analysis (ESCA), (VG Scientific ESCALAB 250). The

dx.doi.org/10.1021/cm1030377 |Chem. Mater. 2011, 23, 2075–2083

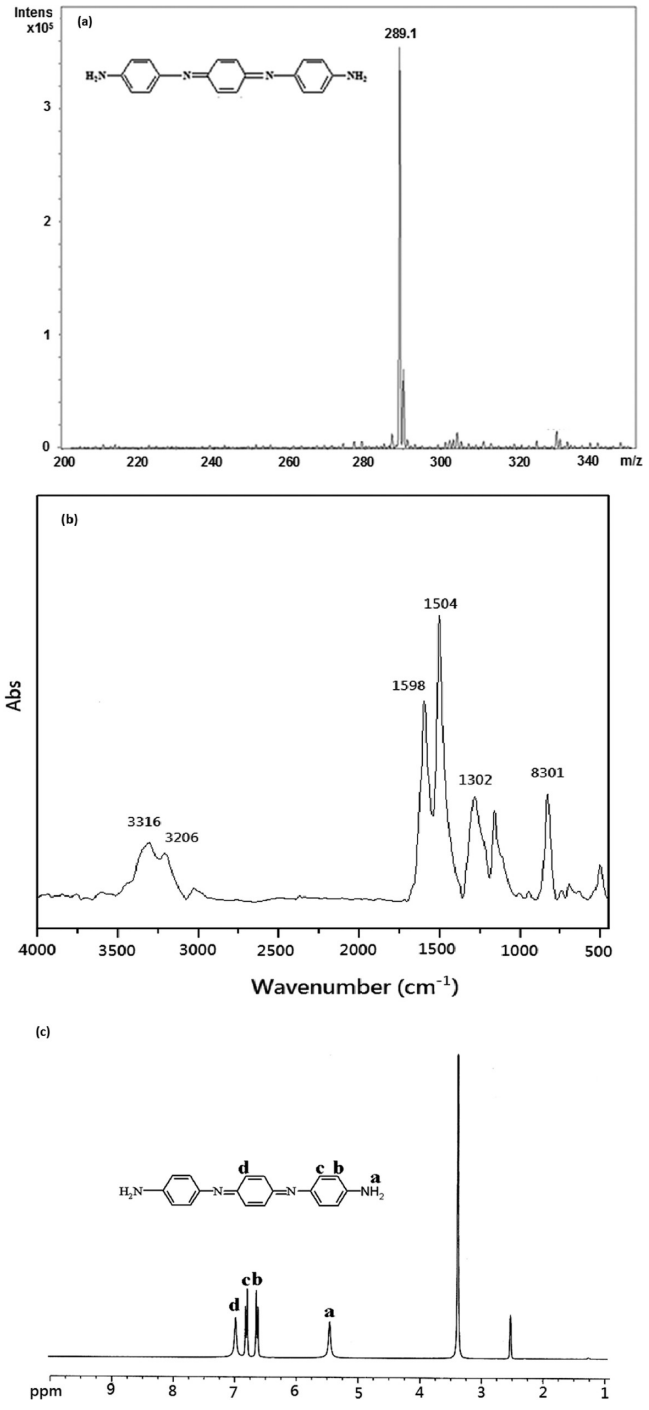

Figure 2. (a) Mass spectrum of AT, (b) FTIR spectrum of AT, and (c) ^{1}H NMR spectrum of AT.

permeation rate was determined by measuring the weight of permeate. Electrochemical measurements were measured by VoltaLab 50. A three-electrode configuration was employed in the circuit with the sample as working electrode, a carbon counter electrode, and a saturated calomel electrode (SCE) as reference electrode. The area of work electrode was 1 cm^2. All the measured potentials presented in the paper were referred to this electrode. All tests were performed at ambient temperature (25 °C) in corrosive medium (3.5 wt % NaCl(aq)). Prior to polarization current (Tafel extrapolation) measurement, 1 h immersion was given to ensure the steady-state. For polarization current experiments, the

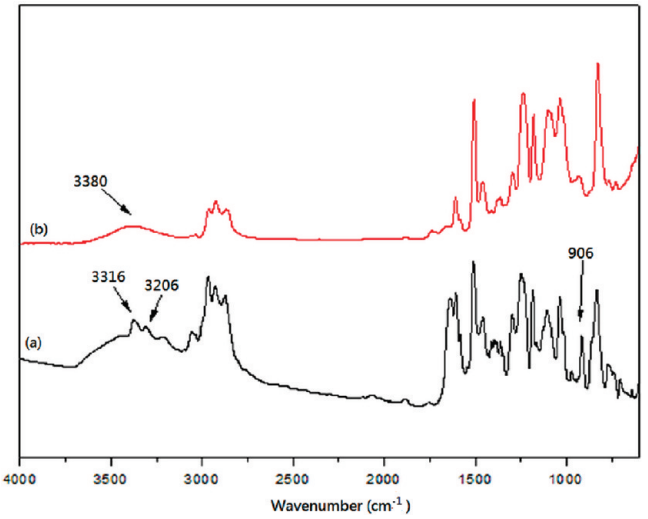

Figure 3. FTIR-ATR spectra of SEE cured with AT and T403 (a) before thermal curing and (b) after thermal curing at 140 °C for 2 h.

potential was scanned from −500 to +500 mV at a scan rate of 1 mV s^{-1}.

Synthesis of Aniline Trimer (AT). 4,4′-Diaminodiphenylamine sulfate (23.65 g, 0.796 mol) and aniline (7.40 g, 0.796 mol) were dissolved in aqueous HCl solution (1.0 M, 800 mL) containing 75 g of NaCl. A solution of ammonium persulfate (18.00 g, 0.789 mol) in aqueous HCl (1.0 M, 200 mL) was added via a dropping funnel into the above solution at −5 °C at the rate of approximately 60 drops/min. The reaction mixture was stirred for 1 h at −5 °C. The resulting precipitate was collected by filtration and washed with aqueous HCl solution (1.0 M, 400 mL) precooled to 0 °C. The solid product was washed with 10% NH_4OH solution (100 mL) and a large amount of distilled water and then dried in a vacuum oven at 50 °C overnight. The aniline trimer (AT) was obtained as a red solid.

Preparation of PDMS Template[32]**.** The PDMS prepolymer was obtained by mixing the elastomer base and curing agent in a proper ratio (10:1, w/w). The prepolymer was poured in molds fixed on a piece of fresh "Xanthosoma Sagittifolium-leaves" and then cured in a 50 °C oven for 4 h. After curing, the PDMS blocks were separated from the molds and used as negative template.

Preparation of Superhydrophobic Electroactive Epoxy (SEE) Coating. The electroactive epoxy resin was prepared by reacting with AT, T-403 and DGEBA. The AT and the T-403 were mixed with DGEBA in suitable amount of DMAc at an epoxy equivalent weight of 0.42:0.43:1 (0.169 g:0.172 g: 0.945 g) for 0.5 h under magnetically stirring at room temperature. Then, drops of the mixture were spread on the cold-rolled steel (CRS), and then the PDMS template was pressed against the mixture surfaces. Then the sample was thermal curing at 50 °C for 1 h, 120 °C for 2 h and 140 °C for 0.5 h. After the curing treatment, the PMDS template was peeled off from the electroactive epoxy coating, the superhydrophobic electroactive epoxy (SEE) coating materials was obtained. The flowchart for the synthesis of SEE was shown in Figure 1.

RESULTS AND DISCUSSION

The typical scheme for the preparation of SEE coating materials by replicating fresh Xanthosoma sagittifolium leaves via a nanocasting technique is given in Figure 1. Oligomeric aromatic amines with amino groups at both ends are of great importance in polymer science and industries because of their applications as model compounds for electroactive polyanilines

and as monomers that are used to prepare polyamides, polyimides, and epoxy polymers. A general one-step approach was recently established by Wei et al. for the synthesis of aniline trimers from inexpensive materials.[10] Accordingly, the trimers could be easily obtained in large quantities by the oxidative coupling of *p*-phenylenediamine and aniline.

Synthesis and Characterization. The molecular weight of AT was characterized by matrix assisted laser desorption ionization time-of-flight mass spectroscopy. Mass spectroscopy is a soft ionization technique affording pseudomolecular ions in the form of M^+ or $(MH)^+$ with little or no fragmentation. From Figure 2a, we can see a molecular ion peak appeared at 289.1, which corresponds to the AT. Moreover, in the FTIR spectrum (Figure 2b) of the AT, the characteristic absorption bands located at 3316 and 3206 cm^{-1} arising from the terminal $-NH_2$ of AT are observed. The characteristic absorption bands appearing at 1598 cm^{-1} and 1504 cm^{-1} were assigned to the vibrational bands of the quinoid rings and benzenoid rings of AT, respectively. For the NMR spectroscopy studies, signals appearing at 5.50 ppm in the ^1H NMR spectrum (Figure 2c) can be assigned to the primary amine protons ($-NH_2$) of AT, and the relative intensity of signals around δ = 7.35−6.50 ppm represents the expected splitting of the aromatic proton signals of AT.[43]

The FT/IR-ATR spectroscopy confirmed the completeness of the curing process of epoxide-ring-opening polymerization reactions between the epoxy ring of DGEBA and the primary amine group of hardener AT and T-403, as indicated by the reduction in the characteristic peaks appearing at 906 cm^{-1} (i.e., epoxy ring)and 3206/3316 cm^{-1} (i.e., primary amine) and the enhancement of the characteristic peaks located at 3380 cm^{-1} (i.e., −OH), as shown in Figure 3.

A photograph image of fresh Xanthosoma Sagittifolium leaves is shown in Figure 4(a). Figure 4b is the higher-magnification SEM image of the Xanthosoma Sagittifolium leaf. The average contact angle on the fresh Xanthosoma Sagittifolium leaves is ca. 146°. From Figure 4b, we can see many small papillary hills on the natural Xanthosoma Sagittifolium leaf. The diameters of the small papillary hills are between 7 and 9 μm. The Xanthosoma sagittifolium leaf-like structure surfaces were fabricated through

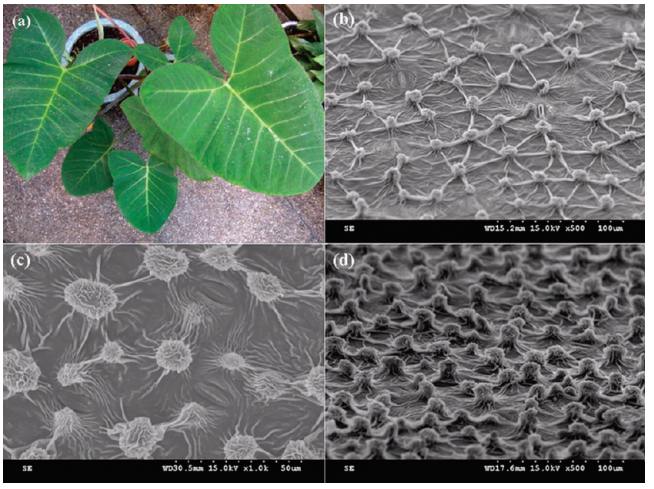

Figure 4. (a) Photograph of the Xanthosoma Sagittifolium leaves. (b) SEM image of the leaf. (c) SEM images of the imprinted layers of SEE showing a top view of the surface. (d) SEM images of the imprinted layers of SEE showing a cross-section view of the surface.

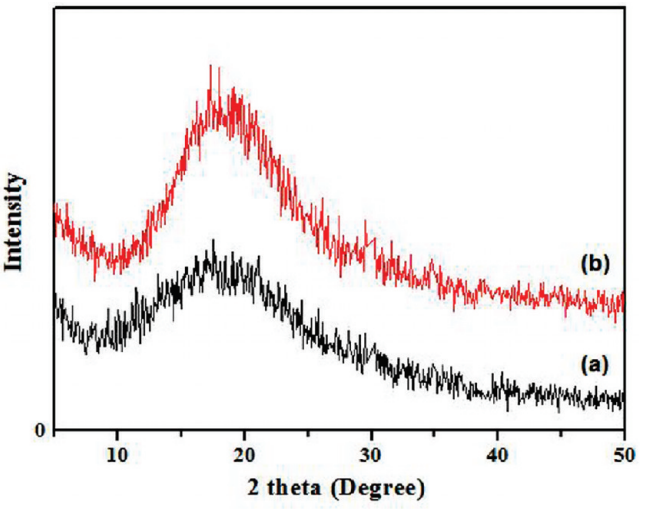

Figure 6. XRD analysis of (a) EE and (b) SEE.

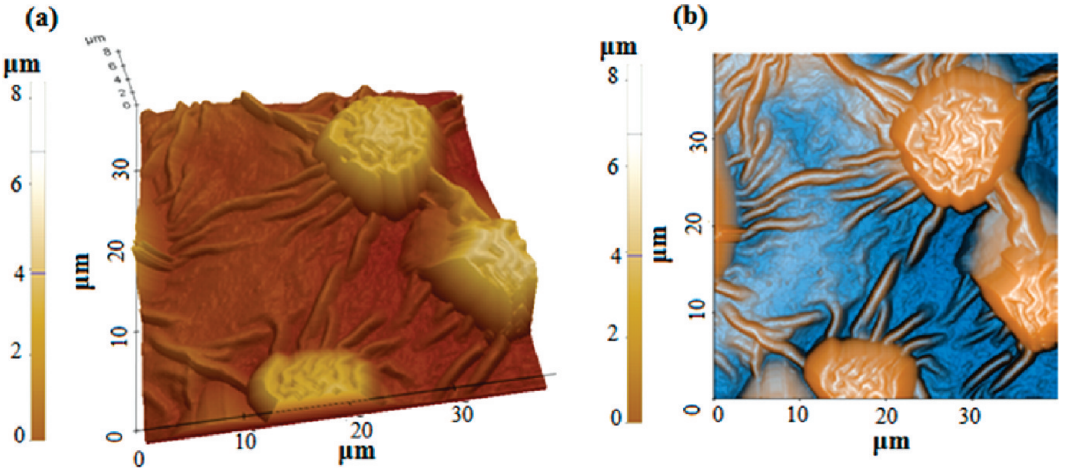

Figure 5. AFM images of the SEE surface topography: (a) two- and (b) three-dimensional.

dx.doi.org/10.1021/cm1030377 |*Chem. Mater.* 2011, 23, 2075–2083

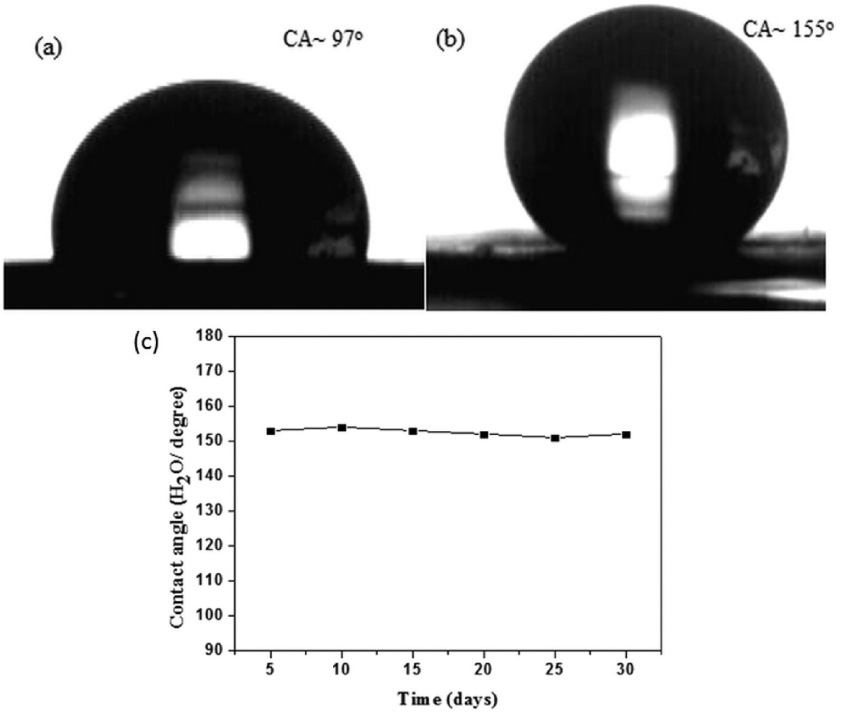

Figure 7. CCD images of the water droplets: (a) EE with CA of 97° and (b) SEE with CA of 155°. (c) Change in water contact angle with time for SEE.

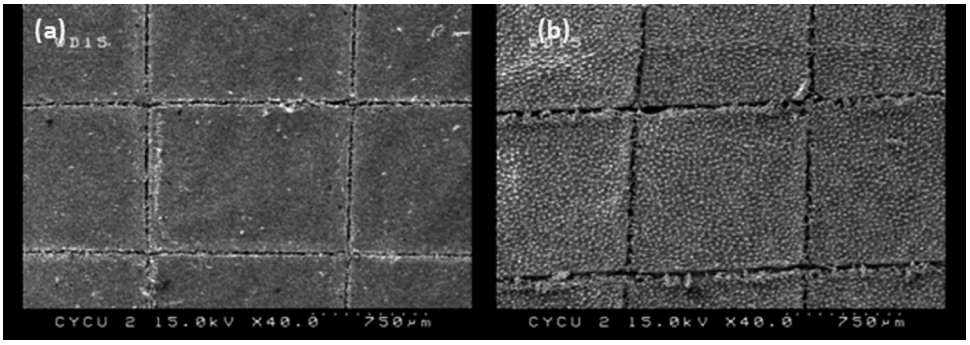

Figure 8. SEM images of (a) EE-coated on CRS and (b) SEE-coated on CRS after testing for adhesion.

replicating the electroactive epoxy polymer using PDMS as a negative template. In this work, an electroactive epoxy resin was used to prepare the ink. Images c and d in Figure 4 show some typical SEM images of the replicated surfaces on the CRS substrate.

In images a and b in Figure 5, the three-dimensional and two-dimensional AFM images of SEE coating on the CRS substrate vividly showed higher surface roughness. It can be seen that papillary nanostructures, which are replicas from the Xanthosoma Sagittifolium leaf, are formed on the surfaces. From the AFM image, the surface morphology is coincident with the SEM observation.

It should be noted that the surface topographic structure on the CRS is complementary with the papillary hills of the natural fresh Xanthosoma Sagittifolium leaf. By using different smooth substrates (such as glass slides or CRS substrates), the resulting surface features are almost the same because the replications are performed on a thin layer that completely covers the substrate surfaces. The PDMS template played a key role in this approach. On account of its low surface energy and good solidification property, the PDMS template could replicate the nanostructures on the Xanthosoma Sagittifolium leaf surface with high fidelity and be easily peeled off without causing obvious damage to the surfaces. In the process, the template was able to retain close contact with the substrate under pressure, which produced the solid nanostructures after replicating.

Figure 6 shows the X-ray diffraction spectrum (XRD) patterns of smooth EE surface and rough SEE surface. The patterns of EE and SEE all show a broadly amorphous peak appearing around 2θ value between 10 and 25° were ascribed to the homogeneously amorphous of electroactive epoxy resin. This result indicates that the nanostructure on the SEE surface replicates from Xanthosoma Sagittifolium leaf cannot influence the degree of crystallinity of electroactive epoxy resin.

This coating material replicated from fresh Xanthosoma Sagittifolium leaf shows superhydrophobic characteristics with a high water contact angle. Images a and b in Figure 7 show the CCD camera images of water droplets on the smooth EE surface

dx.doi.org/10.1021/cm1030377 |*Chem. Mater.* 2011, 23, 2075–2083

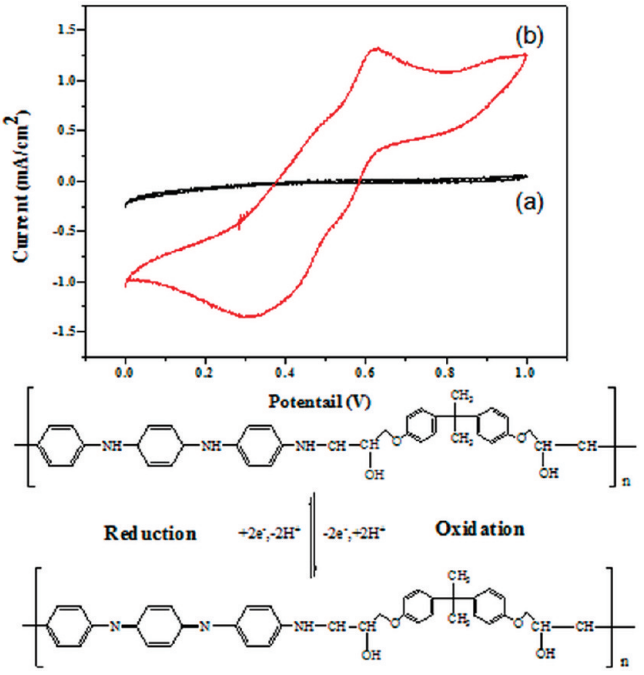

Figure 9. Redox behavior of (a) bare ITO glass, (b) SEE-coated ITO glass electrode measured in 1.0 M H_2SO_4 aqueous solution.

(by spin coating) and Xanthosoma sagittifolium-leaf-like SEE surface on the CRS. The water contact angles of the EE coating and the SEE coating are 97 and 155°, respectively. As shown in Figure 7c, the durability of the water repellent on the SEE coating is a very important issue. The SEE was kept at room temperature in the ambient atmosphere for one month, and water contact angles were measured under each condition, and almost no decrease in water contact angle was observed, indicating that the superhydrophobic property of the as-prepared SEE coating is stable.

In addition, good adhesion between the coating and CRS are essential if the coating is to have effective anticorrosion properties. The adhesion of the EE and SEE coating on the CRS substrate was analyzed according to the cross-cut method.[44] Figure 8 shows SEM images after adhesion tests. There was no significant peeling of either EE or SEE after cross-cutting through the coating. In other words, adhesion between the CRS and both coatings is strong.

As shown in Figure 9, the electrochemical cyclic voltammetric studies indicated that SEE, in the form of the coating, showed a single oxidation peak, which is similar to many longer oligomers that undergo a two electron transfer processes.[45] For example, the SEE had an oxidation current (I_{ox}) of 1.318 mA/cm^2 and a reduction current (I_{red}) of 1.358 mA/cm^2. PANI had been previously reported as an advanced corrosion protection coating material because of its redox catalytic properties of conjugated structures that induce the formation of a passive layer of metal oxide, resulting in effective corrosion protection on various metallic surfaces.[1−5] We therefore envisioned that this redox behavior of as-prepared SEE coatings may probably exhibit a similar enhanced anticorrosive performance as that of PANI, as discussed in the following sections.

The corrosion protection ability of a coating depends on three aspects: (1) water sorption of the coating, (2) transport of water

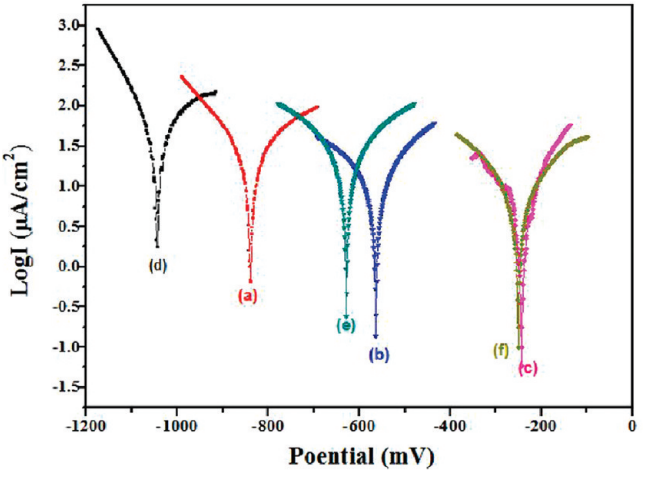

Figure 10. Tafel plots for (a) bare CRS, (b) EE-coated, and (c) SEE-coated electrodes measured in 3.5 wt % NaCl aqueous solution ; (d) bare CRS, (e) EE-coated, and (f) SEE-coated electrodes measured after immersion in 3.5 wt % NaCl aqueous solution for 7days.

in the coating, and (3) accessibility of water to the coating/substrate interface. Therefore, it is reasonable to believe that the SEE with water repellent was able to effectively prevent the water adsorbing onto the substrate surface, and exhibit an superiorcorrosion resistance in the wet environments.

The SEE coating on the CRS electrode was found to be superior based on a series of electrochemical measurements in corrosive medium (3.5 wt % aqueous NaCl electrolyte). Corrosion current information can be obtained by the Tafel extrapolation method, where large cathodic and anodic polarizations provide the cathodic and anodic polarization curves for the respective corrosion processes.[46] Extrapolation of these curves to their point of intersection provides both the corrosion potential and the corrosion current. Corrosion protection studies were performed on samples with 30 ± 1 μm coating thickness immersed in corrosive medium for 1 h. Tafel-plot measurements for the three sample configurations in corrosive medium are shown in Figure 10 and Table 1.

The protection efficiency of the coating has been evaluated using eq 1:[47]

$$\text{protection efficiency } (\%) = \frac{I_{corr} - I_{corr(C)}}{I_{corr}} \times 100 \quad (1)$$

where I_{corr} and $I_{corr(C)}$ are the corrosion current values in the absence and presence of the coating. Tafel plots of the sample-coated CRS electrode measured at an operational temperature of 25 ± 0.5 °C gave a corrosion potential of E_{corr} = −564 mV for the EE coating (Figure 10b), which was found to be more positive than bare CRS (Figure 10a) with E_{corr} = −839 mV. Moreover, the corrosion current (I_{corr}) of the CRS electrode coated with EE was ca. 10.11 μA/cm^2, which was significantly lower than that of bare CRS (i.e., 32.73 μA/cm^2). These results indicated that corrosion protection of EE on CRS substrates results from the formation of passivation oxide layers between polymer and metal surface.

When the Xanthosoma sagittifolium-leaf-like electroactive epoxy surface was treated on the CRS to give a superhydrophobic surface, we found that the corresponding corrosion current (I_{corr}) shifted considerably from 10.11 to 4.33 μA/cm^2

Table 1. Electrochemical Corrosion Measurements and Contact Angle for EE and SEE

sample code	immersion period[b] (day)	pH values[c]	electrochemical corrosion measurements				contact angle (H_2O) (deg)
			E_{corr} (mV)	I_{corr} ($\mu A/cm_2$)	protection efficiency (%)	coating thickness (μm)	
bare[a]	0	7	−839	32.73			72
EE	0	7	−564	10.11	69.11	31	97
SEE	0	7	−244	4.33	86.77	30	155
SEE	0	5	−246	4.39	86.58	30	154
SEE	0	3	−253	4.60	85.94	29	153
SEE	0	1	−259	5.02	84.66	32	153
bare	7	7	−1047	46.88	−43.23	–	<10
EE	7	7	−628	15.58	52.39	31	95
SEE	7	7	−253	4.48	86.31	31	154

[a] Pristine CRS used for test. [b] 3.5% aqueous NaCl electrolyte as an immersion solution . [c] pH values control by 1 M HCl(aq).

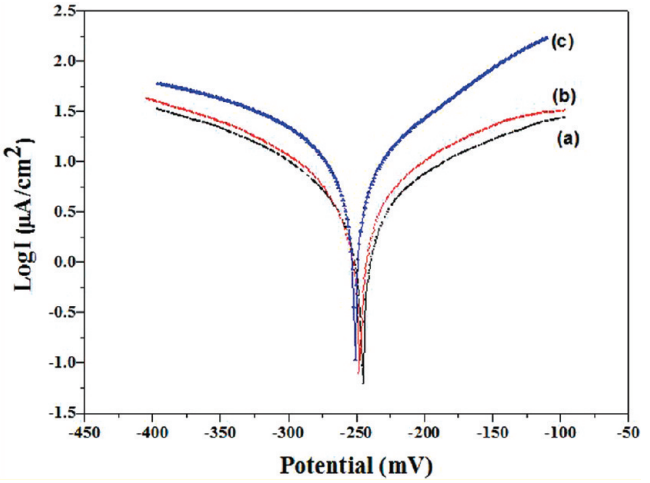

Figure 11. Tafel plots for SEE-coated electrodes measured in (a) pH 5, (b) pH 3, and (c) pH 1 conditions.

under the same conditions. Moreover, corrosion potential (E_{corr}) of CRS electrode coated with SEE (Figure 10c) was found to be better than that of the surface coated with smooth EE. For example, the E_{corr} was found to shift positively from −564 to −244 mV (vs SCE). Comparing the protection efficiency of the smooth EE and SEE coating, the SEE coating showed a protection efficiency value of 86.77%, which was obviously greater than that of smooth EE coating (P_{EF} = 69.11%). On the basis of those electrochemical measurement results, we believe that the SEE coating exhibits corrosion protection on the CRS electrode.

Subsequently, all samples were also recorded after 7 days of immersion in 3.5% NaCl solution by electrochemical corrosion measurements. The comparison of results evidence that the SEE coating (Figure 10f) still presents more positivity E_{corr} (−253 mV) and lower I_{corr} (4.48 $\mu A/cm^2$) than CRS (Figure 10d) and EE (Figure 10e) coating. After immersing 3.5% NaCl solution for 7 days, the I_{corr} of CRS and EE coating significantly increased up from 32.73 and 10.11 $\mu A/cm^2$ to 46.88 and 15.58 $\mu A/cm^2$, respectively. However, the I_{corr} of SEE coating slightly increases up from 4.33 to 4.48 $\mu A/cm^2$. These results show that the SEE coating immersing in corrosive medium for several days still maintains good anticorrosion properties.

Moreover, the Tafel polarization behavior of SEE coating on CRS electrode in different pH conditions (controlled by 1 M HCl) was shown in Figure 11 and Table 1. From the Table 1 it was obviously that the I_{corr} value of SEE coating increases slightly with the pH value decreases from 5 to 1. Even after immersing in the low pH (pH∼1) corrosive medium, the SEE coating still exhibited current density as low as 5.02 $\mu A/cm^2$. We also measured the contact angles of the $HCl_{(aq)}$ droplets (different pH) on the surface of the as-prepared SEE coating. The contact angles of SEE coating still maintained over 150° at different pH condition. As the results, it could be concluded that SEE coating remains good corrosion resistance and high contact angle even in the low pH environment.

Visual observation of the passivation oxide layers revealed the deposition of grayish oxide layer over the CRS surface[7,48] under the SEE coating on the CRS electrode. SEM image studies revealed that the oxide layers were formed at the interface of the SEE coating and the CRS surface (Figure 12b), but we could not observe the same image from bare CRS surface (Figure 12a). In addition to the SEM observations, the chemical nature of the passivation oxide layers was measured by ESCA. All the samples had a two-layer oxide consisting of a Fe_2O_3 layer over a thicker Fe_3O_4 layer.[6,49] The binding energy plots vs intensity for the iron oxide layers are shown in Figure 13a. The passivation oxide layers exhibited the Fe $2p^{3/2}$ peak binding energy of Fe_2O_3 at 710.9 eV, FeO at 709.6 eV, and Fe_3O_4 at 710.3 eV.[49] The Fe 2p spectra of FeO and Fe_3O_4 are similar and it is hard to distinguish them. The $2p^{3/2}$ binding energy was about 724.3 and 710.8 eV. The corrosion protection mechanism of the SEE coatings was attributed to the formation of passivation protective metal oxide layers, induced from the redox catalytic properties of AT that existed in as-prepared SEE coatings, as shown in Figure 13b.

The advanced corrosion protection properties of the SEE coating may have resulted from two possible factors: (a) the redox catalytic property could provide a form of anodic protection between CRS and SEE or (b) the water repellent properties could provide an effective barrier between CRS and its environment. The SEE offered superiorwater repellent properties because of the nanostructure morphology on its surface, which were similar to hills that could easily trap air within the valleys between hills.[25,26] Therefore, the water or Cl^- (in corrosive

dx.doi.org/10.1021/cm1030377 |Chem. Mater. 2011, 23, 2075–2083

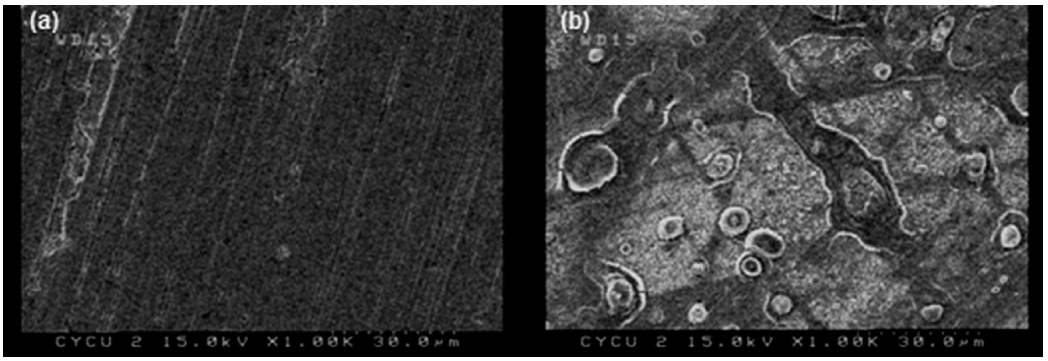

Figure 12. SEM image for (a) polished CRS metal, and the surface of the (b) SEE coating and the CRS metal.

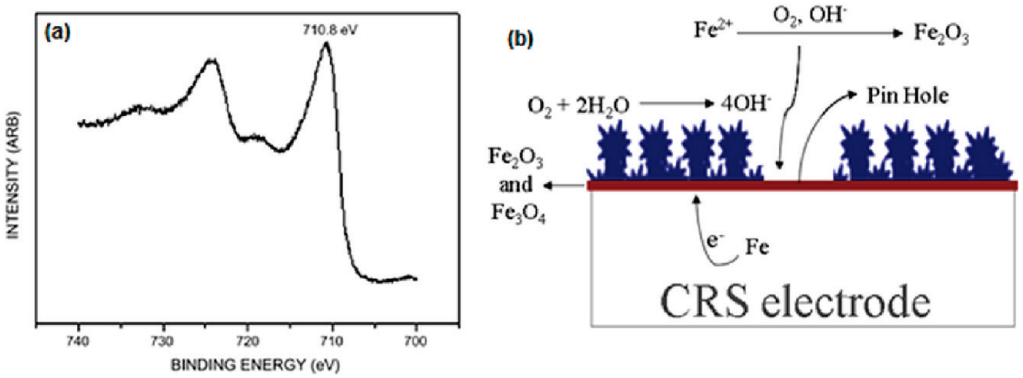

Figure 13. (a) ESCA Fe 2p core level spectra of SEE. (b) Schematic diagram of mechanism of CRS passivation by SEE coatings.

medium) can hardly reach the under coating of the CRS due to the obstructive effect of air valleys. Therefore, there are two ways in which this coating could indirectly prevent corrosive damage. SEE has excellence anticorrosion properties, and is superior to the bare CRS electrode and EE coated CRS electrode.

CONCLUSIONS

In conclusion, we have shown the preparation of advanced anticorrosion coating materials from electroactive epoxy; these materials synergistically repel water and have enhanced redox catalytic capability. The SEE coating provides superiorcorrosion protection of the coated CRS substrate and provides an effective barrier to aggressive species. The enhancement of the corrosion protection of SEE coated on the CRS electrode could be interpreted by the following two possible reasons: (a) electroactive epoxy provided a form of anodic protection that significantly reduced corrosion rates in corrosive medium and/or (b) the water repellent property provided a water barrier in the coating surface. Since this fabrication method is simple, easy to control, and highly faithful to the structure of the original template even on the nanoscale, it is believed that this conception should be easily applied to large-scale production of SEE materials with commercial application in the corrosion protection of CRS.

AUTHOR INFORMATION

Corresponding Author

*E-mail: juiming@cycu.edu.tw. Tel: +886-3-2653340. Fax: +886-3-2653399.

ACKNOWLEDGMENT

The financial support of this research by the Ministry of Education, Taiwan, R. O. C., NSC 98-2113-M-033-001-MY3, and department of chemistry at CYCU,CYCU-98-CR-CH, are gratefully acknowledged.

REFERENCES

(1) McAndrew, T. P.; Miller, S. A.; Gilicinski, A. G.; Robeson, L. M. *Polym. Mater. Sci. Eng.* **1996**, *74*, 204.
(2) Wessling, B.; Posdorfer, J. *Electrochim. Acta* **1999**, *44*, 2139.
(3) Kinlen, P. J.; Silverman, D. C.; Jeffreys, C. R. *Synth. Met.* **1997**, *85*, 1327.
(4) Camalet, J. L.; Lacroix, J. C.; Aeiyach, S.; Chaneching, K.; Lacaze, P. C. *Synth. Met.* **1998**, *93*, 133.
(5) DeBerry, D. W. *J. Electrochem. Soc.* **1985**, *132*, 1022.
(6) Wessling, B. *Adv. Mater.* **1994**, *6*, 226.
(7) Talo, A.; Passiniemi, P.; Forsen, O.; Ylasaari, S. *Synth. Met.* **1997**, *85*, 1333.
(8) Spinks, G. M.; Dominis, A. J.; Wallace, G. G.; Tallman, D. E. *J. Solid State Electrochem.* **2002**, *6*, 85.
(9) Li, P.; Tan, T. C.; Lee, J. Y. *Synth. Met.* **1997**, *88*, 237.
(10) Wang, Z. Y.; Yang, C.; Gao, J. P.; Lin, J.; Meng, X. S.; Wei, Y.; Li, S. *Macromolecules* **1998**, *31*, 2702.
(11) Lu, W.; Meng, X. S.; Wang, Z. Y. *J. Polym. Sci., Part A: Polym. Chem.* **1999**, *37*, 4295.
(12) Chao, D.; Cui, L.; Lu, X.; Mao, H.; Zhang, W. J.; Wei, Y. *Eur. Polym. J.* **2007**, *43*, 2641.
(13) Chao, D.; Lu, X.; Chen, J.; Zhao, X.; Wang, L.; Zhang, W. J.; Wei, Y. *J. Polym. Sci., Part A: Polym. Chem.* **2006**, *44*, 477.

(14) Chao, D.; Ma, X.; Lu, X.; Cui, L.; Mao, H.; Zhang, W. J.; Wei, Y. *Macromol. Chem. Phys.* **2007**, *208*, 658.
(15) Chao, D.; Ma, X.; Lu, X.; Cui, L.; Mao, H.; Zhang, W. J.; Wei, Y. *J. Appl. Polym. Sci.* **2007**, *104*, 1603.
(16) Chao, D.; Lu, X.; Chen, J.; Liu, X.; Zhang, W. J.; Wei, Y. *Polymer* **2006**, *47*, 2643.
(17) Chen, L.; Yu, Y.; Mao, H.; Lu, X.; Yao, L.; Zhang, W.; Wei, Y. *Polymer* **2005**, *46*, 2825.
(18) Huang, K. Y.; Shiu, C. L.; Wu, P. S.; Wei, Y.; Yeh, J. M.; Li, W. T. *Electrochimi Acta* **2009**, *54*, 5400.
(19) Huang, K. Y.; Jhuo, Y. S.; Wu, P. S.; Lin, C. H.; Yu, Y. H.; Yeh, J. M. *Eur. Poly. J.* **2009**, *45*, 485.
(20) Neinhuis, C.; Barthlott, W. *Ann. Bot.* **1997**, *79*, 667.
(21) Claugher, D 1990 *Scanning Electron Microscopy in Taxonomy and Functional Morphology*; Oxford: Clarendon, U.K., pp 69−94.
(22) Barthlott, W.; Neinhuis, C. *Planta* **1997**, *202*, 1.
(23) Furstner, R.; Barthlott, W.; Neinhuis, C.; Walzel, P. *Langmuir* **2005**, *21*, 956.
(24) Otten, A.; Herminghaus, S. *Langmuir* **2004**, *20*, 2405.
(25) Liu, T.; Yin, Y.; Chen, S.; Chang, X.; Cheng, S. *Electrochim. Acta* **2007**, *52*, 3709.
(26) Liu, T.; Chen, S.; Cheng, S.; Tian, J.; Chang, X.; Yin, Y. *Electrochim. Acta* **2007**, *52*, 8003.
(27) Erbil, H. Y.; Demirel, A. L.; Avc, Y.; Mert, O. *Science* **2003**, *299*, 1377.
(28) Feng, L.; Song, Y.; Zhai, J.; Liu, B.; Xu, J.; Jiang, L.; Zhu, D. *Angew. Chem. Int. Edn* **2003**, *42*, 800.
(29) Feng., X.; Feng, L.; Jin, M.; Zhai, J.; Jiang, L.; Zhu, D. *J. Am. Chem. Soc.* **2004**, *126*, 62.
(30) Woodward, I.; Schofield, W. C. E.; Roucoules, V.; Badyal, J. P. S. *Langmuir* **2003**, *19*, 3432.
(31) Shui, J.; Kuo, C.; Chen, P.; Mou, C. *Chem. Mater.* **2004**, *16*, 561.
(32) Lee, W.; Jin, M.; Yoo, W.; Lee, J. *Langmuir* **2004**, *20*, 7665.
(33) Zhao, X.; Li, W. *Surf. Coat. Technol.* **2006**, *200*, 3492.
(34) Han, J. T.; Xu, X.; Cho, K. *Langmuir* **2005**, *21*, 6662.
(35) Xie, Q.; Fan, G.; Zhao, N.; Guo, X.; Xu, J.; Dong, J.; Zhang, L.; Zhang, Y.; Han, C. C. *Adv. Mater.* **2004**, *16*, 1830.
(36) Chen, W.; Fadeev, A. Y.; Hsieh, M. C.; Ö ner, D.; Youngblood, J.; McCarthy, T. J. *Langmuir* **1999**, *15*, 3395.
(37) Zhang, J.; Li, J.; Han, Y. *Macromol. Rapid Commun.* **2004**, *25*, 1105.
(38) Li, Y.; Cai, W.; Duan, G.; Cao, B.; Sun, F.; Lu, F. *J. Colloid Interface Sci.* **2005**, *287*, 634.
(39) Khorasani, M. T.; Mirzadeh, H.; Kermani, Z. *Appl. Surf. Sci.* **2005**, *242*, 339.
(40) Yabu, H.; Takebayashi, M.; Tanaka, M.; Shimomura, M. *Langmuir* **2005**, *21*, 3235.
(41) Wu, X.; Zheng, L.; Wu, D. *Langmuir* **2005**, *21*, 2665.
(42) Wu, X.; Shi, G. *Nanotechnology* **2005**, *16*, 2056.
(43) Wei, Y.; Yang, C.; Ding, T. *Tetrahedron Lett.* **1996**, *37*, 731.
(44) Beving, D. E.; McDonnell, A. M. P.; Yang, W. S.; Yan, Y. S. *J. Electrochem. Soc.* **2006**, *153*, B32.
(45) Chen, R.; Benicewicz, B. C. *Macromolecules* **2003**, *36*, 6333.
(46) (a) Mitra, A.; Wang, Z. B.; Cao, T. G.; Wang, H. T.; Huang, L. M.; Yan, Y. S. *J. Electrochem. Soc.* **2002**, *149*, B472. (b) Beving, D. E.; McDonnell, A. M. P.; Yang, W. S.; Yan, Y. S. *J. Electrochem. Soc.* **2006**, *153*, B325. (c) Cheng, X. L.; Wang, Z. B.; Yan, Y. S. *Electrochem. Solid-State Lett.* **2001**, *4*, B23.
(47) Kamaraj, K.; Karpakam, V.; Sathiyanarayanan, S.; Venkatachari, G. *Mater. Chem. Phys.* **2010**, *122*, 123.
(48) Wessling, B. *Mater. Corros.* **1996**, *47*, 439.
(49) Fahlman, M.; Jasty, S.; Epstein, A. J. *Synth. Met.* **1997**, *85*, 1323.